SEG 2014 benchmark data

Ali Almomin, Xukai Shen, Carlo Fortini, Guillaume Barnier and Biondo Biondi

ABSTRACT

A synthetic bunchmark test data was created by Chevron for the SEG 2014 workshop. We first overview the data and the potential challenges that it presents for velocity estimation methods. Then, we process the data by reducing the noise and the sea bed surface-related multiples. Finally, we estimate the P-wave velocity model with a sequence of full waveform inversion methods that first analyze the early arrivals then the reflection data. The angle-domain common-image gathers of the final velocity model show significant improvement compared to the initial velocity model and indicate that most of the kinematics of the data were successfully estimated.

INTRODUCTION

Full waveform inversion (FWI)(Tarantola, 1984; Pratt, 1999) has become an increasingly popular technique to estimate the subsurface property from seismic data due to its high resolution and very accurate results. This high resolution is due to utilizing the information from both the forward-scattered and back-scattered wavefields in the data, i.e. both their kinematics and their dynamics. Moreover, the data misfit is computed in the data spaces. This direct computation of the errors results in a relatively simple relationship between the data residuals and the model updates. However, FWI has the disadvantage that its objective function is far from being smooth and convex which, in the absence of very low frequency, requires the starting model to be very close to the true model to avoid converging to a local minimum.

To test and compare different FWI algorithms, Chevron has recently released a benchmark synthetic dataset for a blind test as part of the SEG 2014 workshop. The data are modeled based on real geology and present several challenges that can prevent a conventional implementation of FWI from working properly.

We reduce the noise in the data by applying a bandpass filter followed by a multiples reduction algorithm that targets sea bed surface related multiples. To estimate the P-wave velocity model, we first run an early arrival full waveform inversion to estimate the shallow part of the model. Then, we run a low frequency tomographic full waveform inversion (TFWI) (Almomin and Biondi, 2014) on the reflection data to improve the background velocity at the deeper part of the data. Finally, we run a kinematics based FWI on the reflection data. The angle-domain common-image gathers of the final velocity model show significant improvement compared to the initial

velocity model and indicate that most of the kinematics of the data were successfully estimated.

DATA OVERVIEW

The dataset was modeled using a 2D isotropic, elastic wave-equation with a free-surface at top and absorbing boundaries on the sides and the bottom. The source function used was provided as a farfield wholespace wavelet without ghosts effects with a sampling rate of 0.666666 ms. Figure 1 shows the wavelet provided and figure 2 shows the amplitude spectrum of the wavelet, which shows a majority of the signal between 2 Hz and 40 Hz with a dominant frequency of 10 Hz. A marine geometry was used with 1600 shots separated by 25 m and 321 hydrophone receivers separated by 25 m. The receivers start at the source location and reach a maximum of 8000 m. Both sources and receivers are at a depth of 15 m. The recorded data had a duration of 8 s with a sampling of 4 ms.

Figure 3 shows the first shot gather and figure 4 shows the zero-offset gather of the raw data, which show the source and receiver ghosts effects and the free-surface multiples. Moreover, noise was added to the data that mostly affects the very low and very high ends of the frequency spectrum. The noise can be seen in the amplitude spectrum of the first shot gather in figure 5 as well as the average amplitude spectrum of all shot gathers in figure 6, which was obtained by first computing the amplitude spectrum of each shot then averaging those spectra.

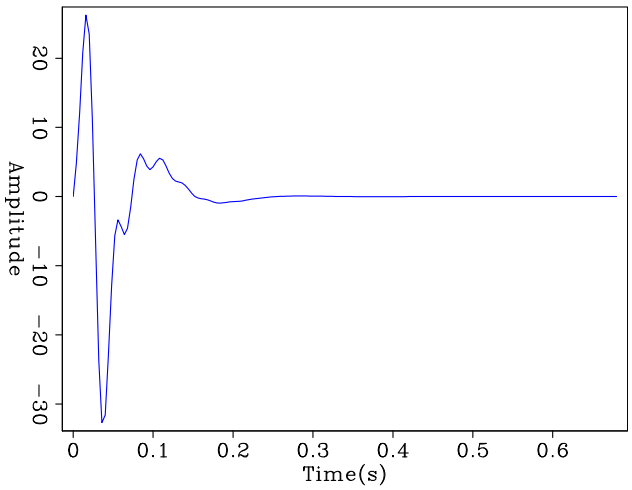

Figure 1: Source wavelet. [**ER**]

MULTIPLES REDUCTION

The original data was modeled with an elastic FD algorithm with a free-surface boundary condition in order to simulate the presence of surface-related multiples. The first layer of the model is constituted by water. The surface-related multiple

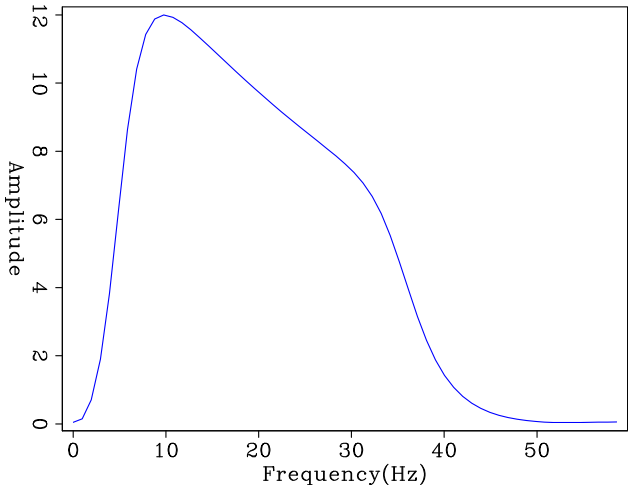

Figure 2: Amplitude spectrum of the source wavelet. [**ER**]

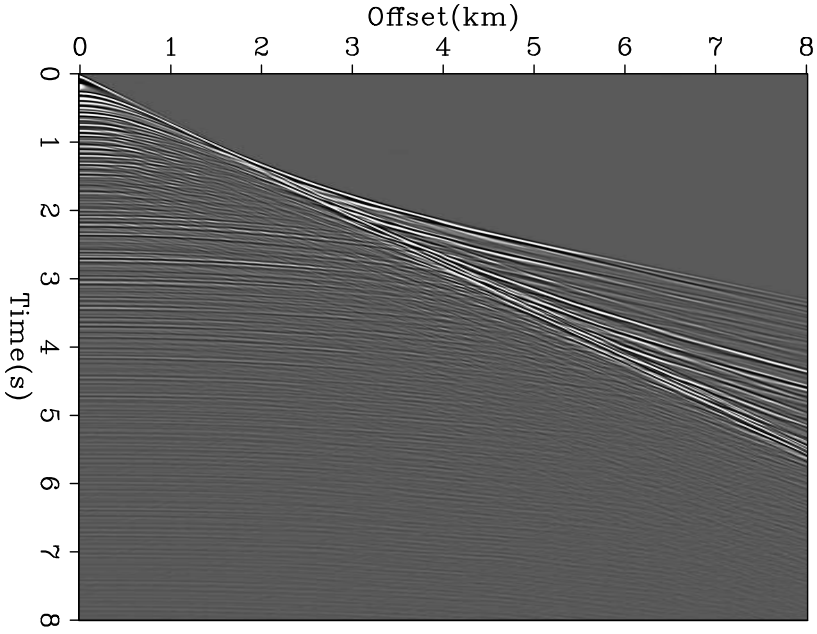

Figure 3: First shot gather of the raw data. [**ER**]

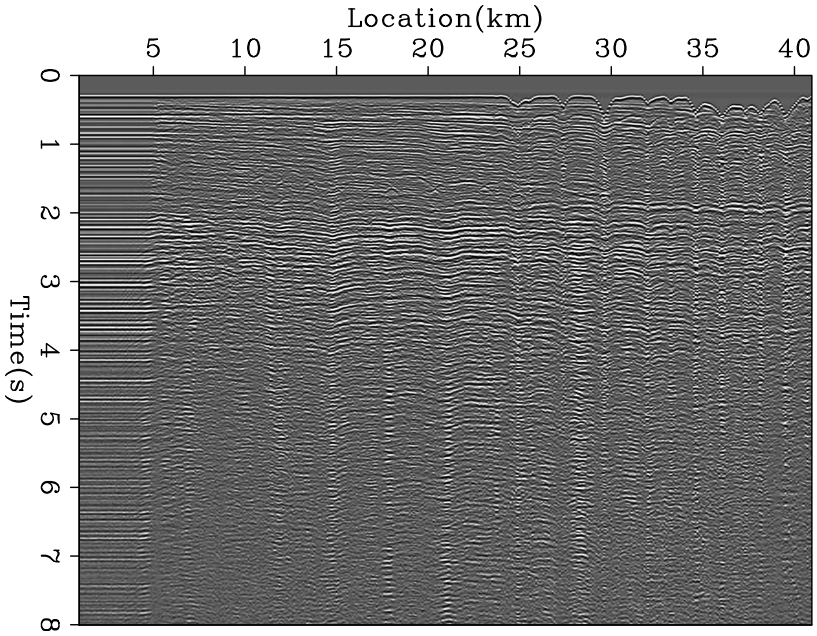

Figure 4: Zero offset gather of the raw data. [**ER**]

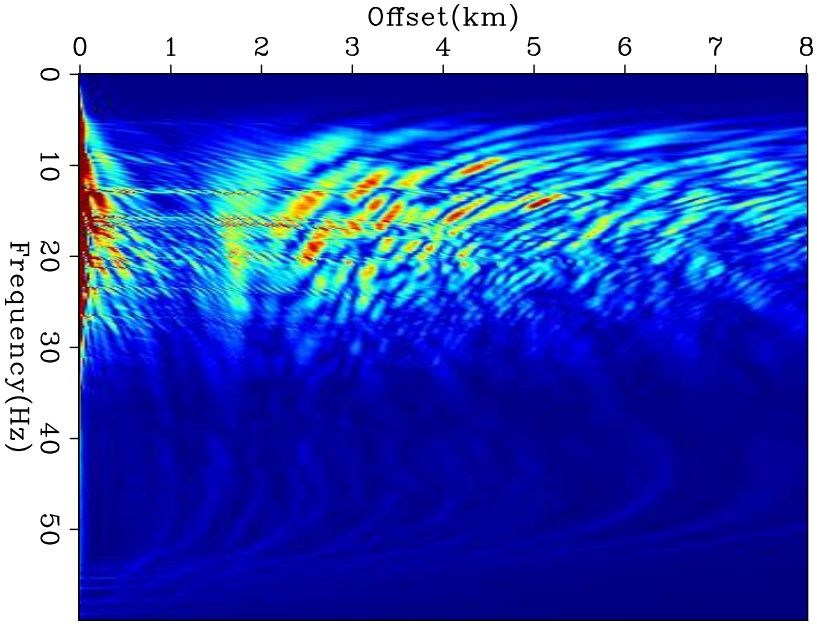

Figure 5: Amplitude spectrum of the first shot gather of the raw data. [**ER**]

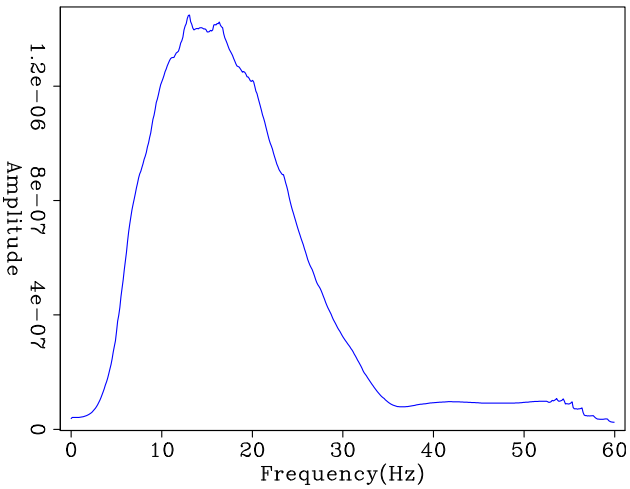

Figure 6: Average amplitude spectrum of all shot gathers of the raw data. [**ER**]

events that underwent to, at least a bounce, at the depth of the seabed seem to be the most energetic ones.

In order to remove the multiples from the original data, we applied a model-based prediction algorithm that generates a model of the seabed surface-related multiples (noise model). We then adaptively subtracted the noise model from the original data with a 2D Least Squares adaptive subtraction filter.

The model-based algorithm we used is called MRKE (Multiple Removal by Kirchhoff Extrapolation). It needs as input an interpreted reflector and the velocity model between the acquisition surface and that reflector. By using a Kirchhoff wavefield extrapolation operator, the algorithm simulates the additional bounce of the primary events recorded in the data that occurred at the depth of the reflector. This way, the primaries contained in the data are transformed into multiples (and the multiples in higher order multiples). Since the same operation is applied on all the events in the original data, also the receiver-side peg-legs of the interpreted reflector are predicted. The source-side peg-legs can also be predicted by applying the same algorithm after a re-ordering of the input data in common-receiver gathers (CRGs).

Here are the steps we followed for the removal of the multiples from the original data:

1) Picking of the seabed interface from the given initial velocity model
2) MRKE on the original data
3) MRKE on the original data re-sorted in CRGs
4) Merge of the results of steps 2) and 3)
5) Adaptive subtraction of the predicted multiples from the original dataset

Figure 7 shows the first shot gather after removing the multiples. By comparing figure 7 to figure 3, we can see that several events, most notably around early time

and far offset, have been removed. Figure 8 shows the amplitude spectrum of the shot gather shown in figure 7. Figure 9 shows the zero-offset gather with a t-power gain using an exponent value of one. Finally, figure 10 shows the average amplitude spectrum of all shot gathers, which was obtained by first computing the amplitude spectrum of each shot then averaging those spectra.

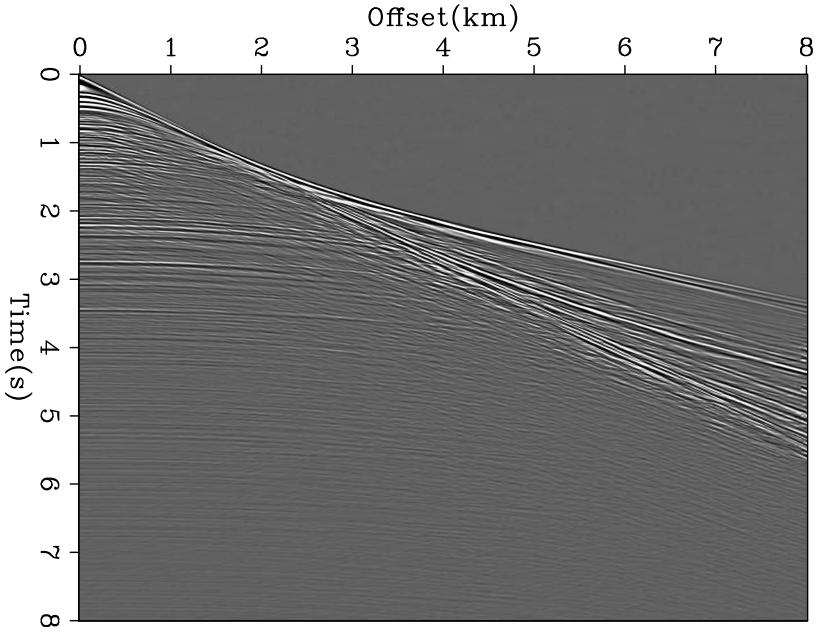

Figure 7: First shot gather of the de-multipled data. [**NR**]

VELOCITY ANALYSIS

Initial velocity

A 1-D initial velocity model was provided with the data that contains the sea bottom and a water velocity of 1.51 km/s, as shown in figure 11. The left side of the model has a flat sea bottom whereas the right side has more complex topography. The first shot is located at 1 km with the receivers extending towards the right.

For all subsequent steps, we reduce the computational cost by subsampling the source function to a rate of 4 ms, matching the sampling of the recorded data, and the source spacing to a rate of 100 m spacing by keeping every fourth shot gather. We also applied a bandpass filter with parameters 2-4-35-40 Hz to reduce the low- and high-frequency noise. Moreover, we symmetrize around common-midpoint (CMP) locations using reciprocity in order to produce image and angle-gathers that are easier to interpret.

Figure 12 shows the migration image obtained using the initial velocity model and the demultipled data after muting the early arrivals. The events are very incoherent and defocused due to large velocity errors. Figure 13 shows the angle-domain

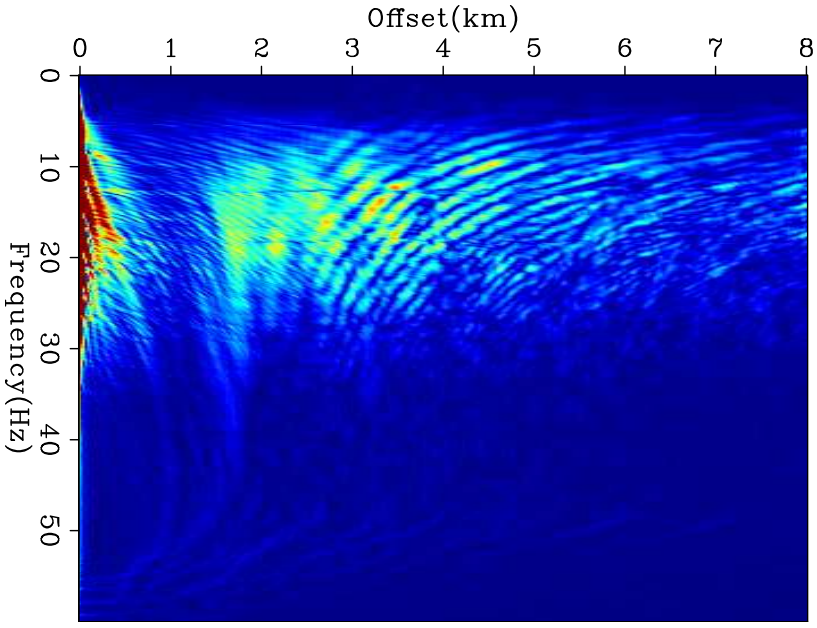

Figure 8: Amplitude spectrum of the first shot gather of the de-multipled data. [**NR**]

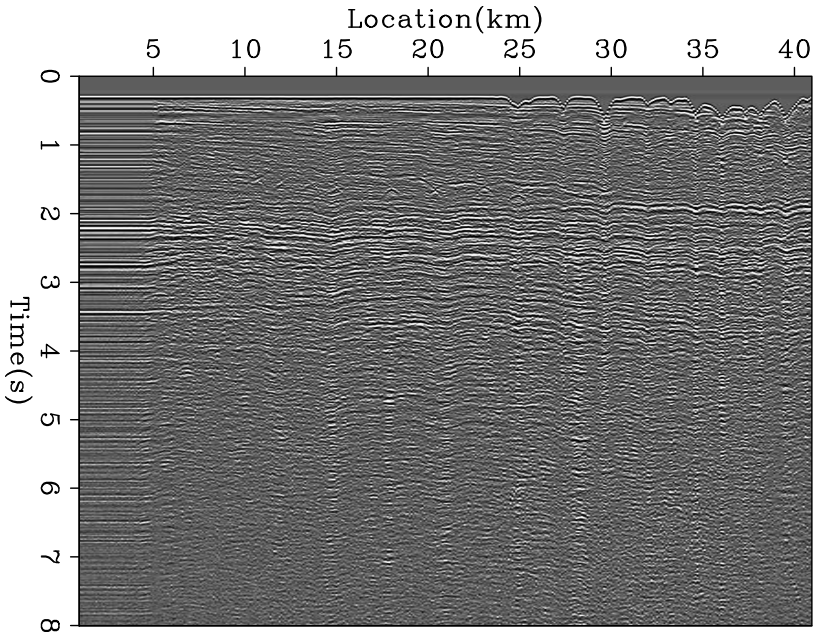

Figure 9: Zero offset gather of the de-multipled data. [**NR**]

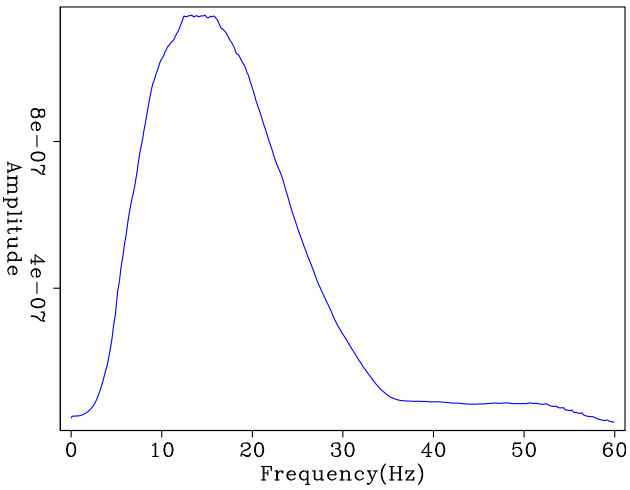

Figure 10: Average amplitude spectrum of all shot gathers of the de-multipled data. [**NR**]

common-image gathers (ADCIGs) using the initial velocity model. The ADCIGs have 13 equally spaced gathers starting at a location of 10 km and ending at 40 km with an opening angle range between -50 to +50 degrees. The gathers show strong curvature as we go towards the right side and the deep part of the model, indicating significant velocity errors in the model.

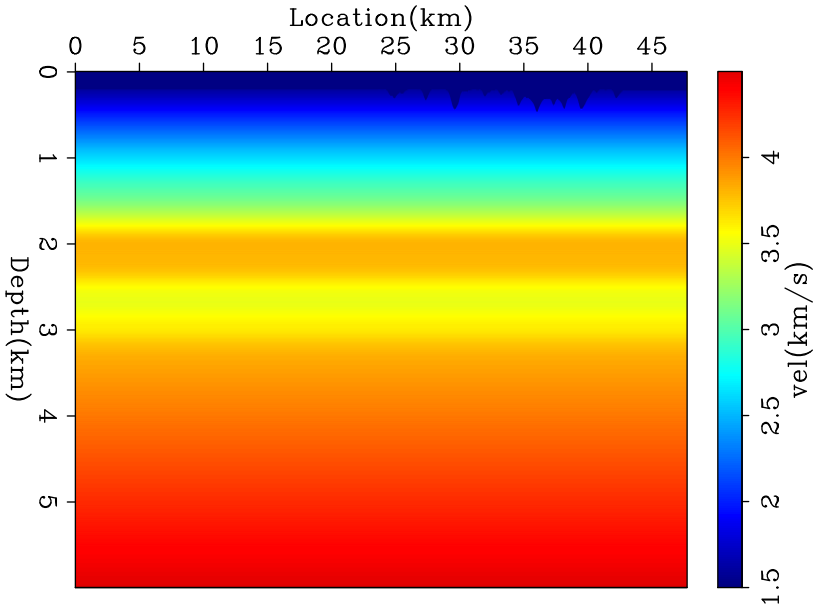

Figure 11: Initial velocity model. [**ER**]

Early arrival FWI

The long-offset shot gathers provide an excellent opportunity for deriving the near-surface velocity model using early-arrival waveform inversion. The recorded data have

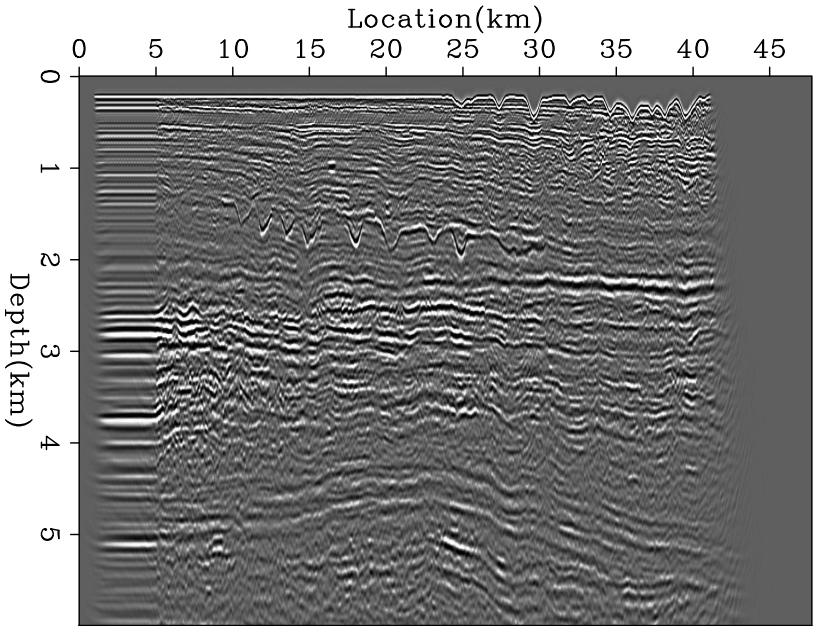

Figure 12: Migration image using the initial velocity model. [**NR**]

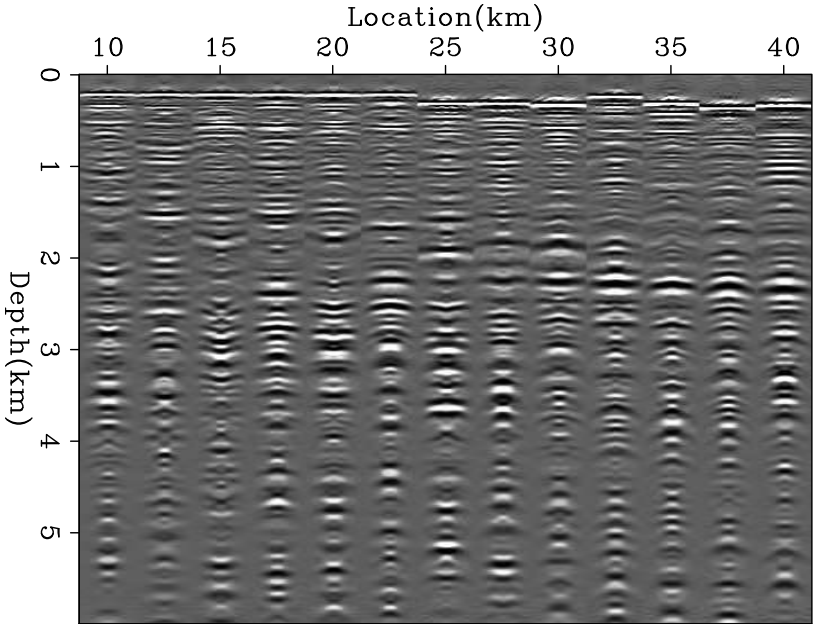

Figure 13: ADCIGs using the initial velocity model. [**NR**]

offset up to 8 km, which allow us to estimate velocity down to about 2 km. The near-surface velocity estimation was performed using a workflow described in (Shen et al., 2012). Using first-breaks only, wave-equation traveltime inversion (Woodward, 1989; Luo and Schuster, 1991) was performed, using the preprocessed data with bandpass between 5 Hz and 10 Hz. After that, using early-arrivals with the same bandpass parameters as observed data, Kinematic Waveform Inversion (KWI)(Shen, 2014) was performed.

The final result of the workflow in figure 14 shows significant improvement of the near-surface velocity model. Not only does the migrated image have much better lateral coherency (figure 15), but also does the angle gathers (figure 16) become much flatter

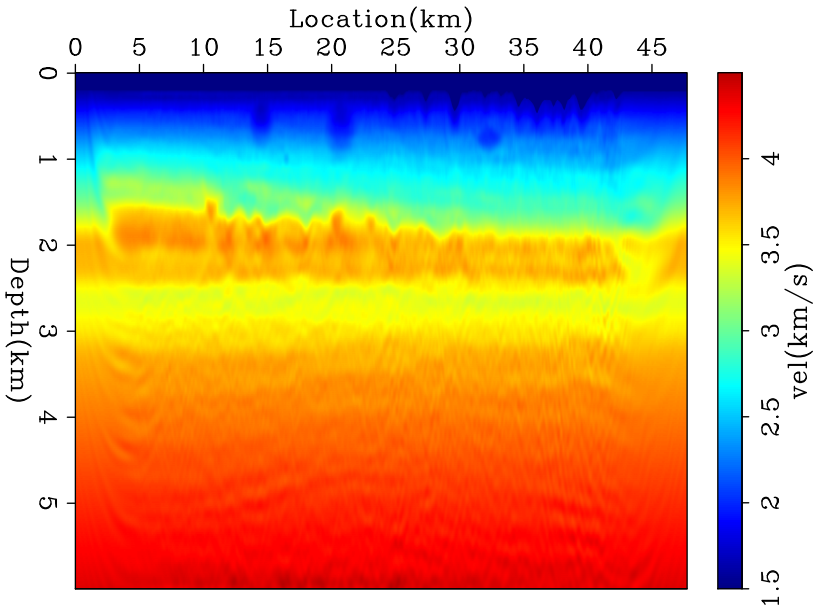

Figure 14: Early-arrival FWI velocity model. [**NR**]

Low frequency TFWI

The next step is to extract the kinematic information from the reflection data. We follow the strategy suggested by Biondi and Almomin (2014) by doing a two-stage inversion. First, we ran TFWI on the low frequency part of the data (up to 10 Hz) with strong regularization. Second, we run FWI starting from the low-frequency TFWI results. The regularization used in TFWI can be equivalently applied as a pre-conditioning to the gradient. The preconditioner strongly smooths in the horizontal direction and slightly in the vertical direction. The preconditioning also helps avoiding overfitting the amplitude, which is undesirable in this case due to the fact that we use an acoustic wave-equation on data modeled with an elastic wave-equation.

The output of running low-frequency TFWI is shown in figure 17. There is a

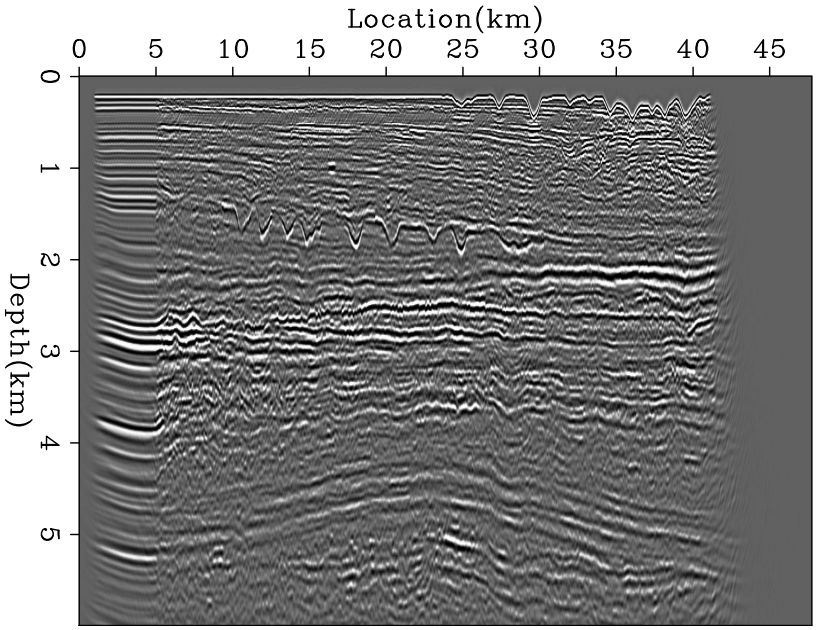

Figure 15: Migration image using the early-arrival FWI velocity model. [**NR**]

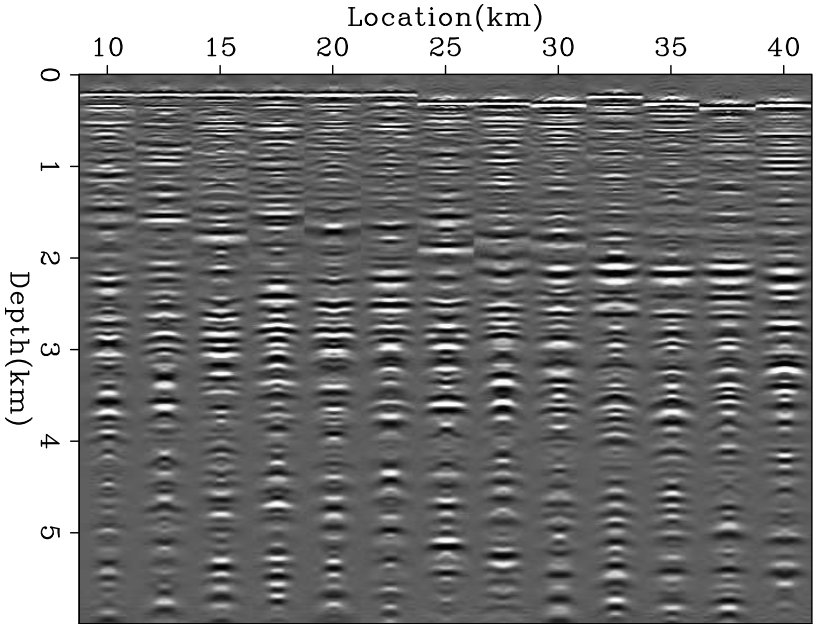

Figure 16: ADCIGs using the early-arrival FWI velocity model. [**NR**]

significant decrease in velocity between 2.5 km and 3.5 km depths and an increase in velocity below that. Also, a slow-velocity anomaly shows up around 28 km in the horizontal coordinate and 2.8 km depth. The migration image using the low-frequency TFWI is shown in figure 18, which shows a large improvement in reflectors continuity and amplitude compared to figure 15, indicating better overall focusing of the events. The improvement in velocity is also validated by flatness of reflectors as shown in figure 19.

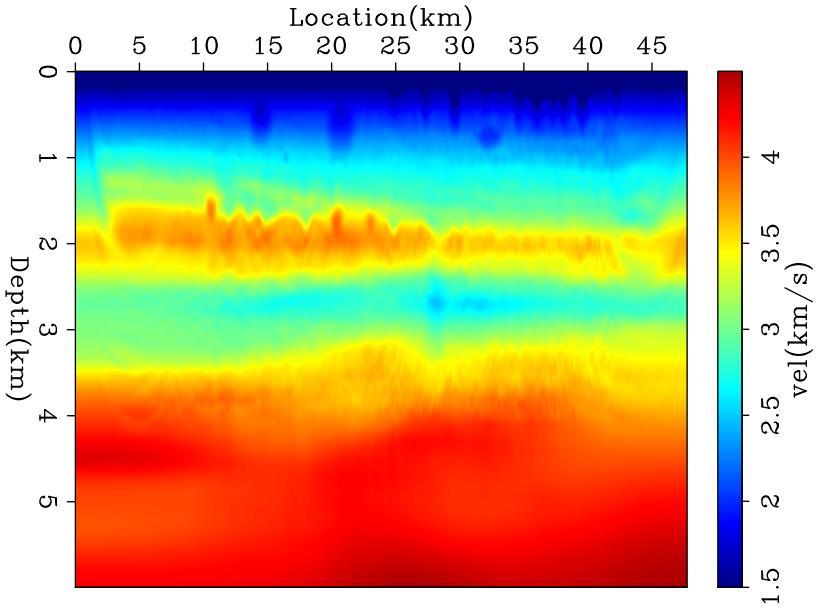

Figure 17: Low-frequency TFWI velocity model. [**NR**]

Reflection FWI

Next, waveform inversion was performed using the TFWI result as the starting model. Since early arrivals had been used to derive the near-surface velocity model, and the near-surface model almost did not change after TFWI, those early-arrivals were not used in the waveform inversion here. In other words, only reflections were used as the observed data. Consequently, the final result after waveform inversion (Figure 20) has a lot of details of the reflectors, especially after 2.5 km depth, where the previous early-arrival waveform inversion failed to update due to limited illumination. Thanks to the long-wavelength components updated from TFWI, the reflection waveform inversion was able to update the short wavelength components of the model. This is verified by better focusing of the migrated image (Figure 21) and better flattened angle gathers (Figure 22).

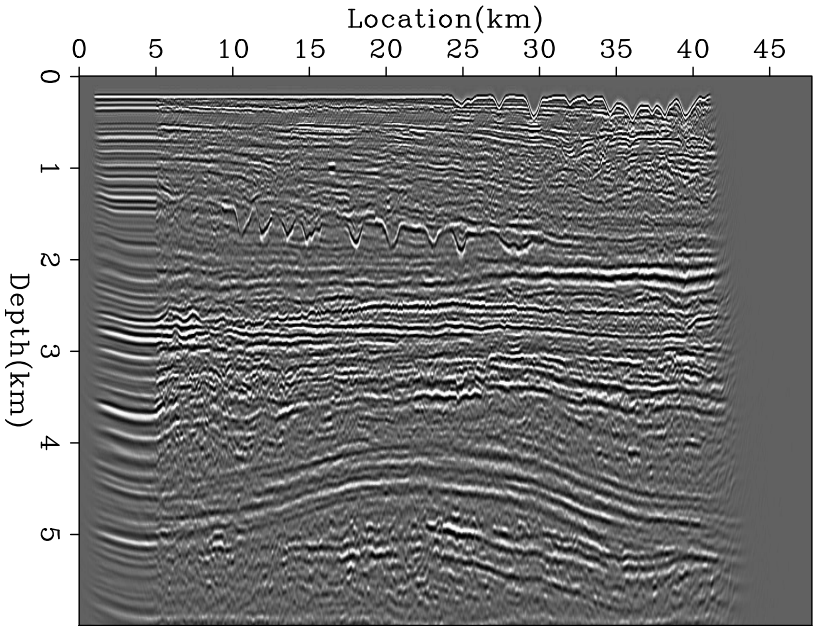

Figure 18: Migration image using the low-frequency TFWI velocity model. [**NR**]

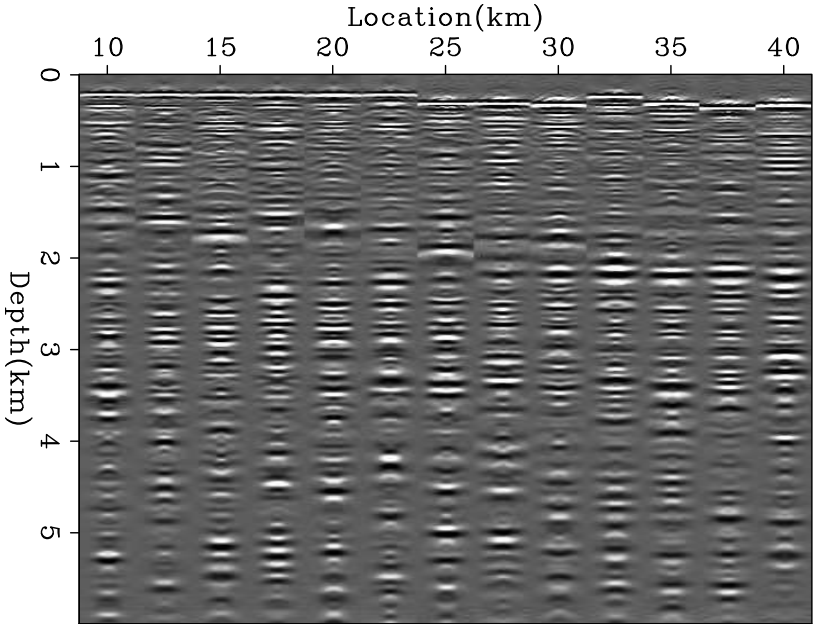

Figure 19: ADCIGs using the low-frequency TFWI velocity model. [**NR**]

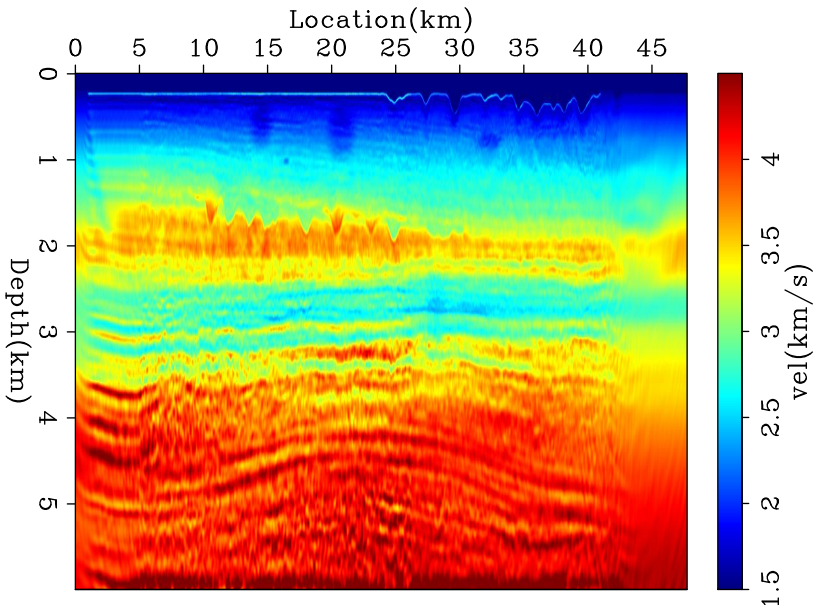

Figure 20: Reflection FWI velocity model. [**NR**]

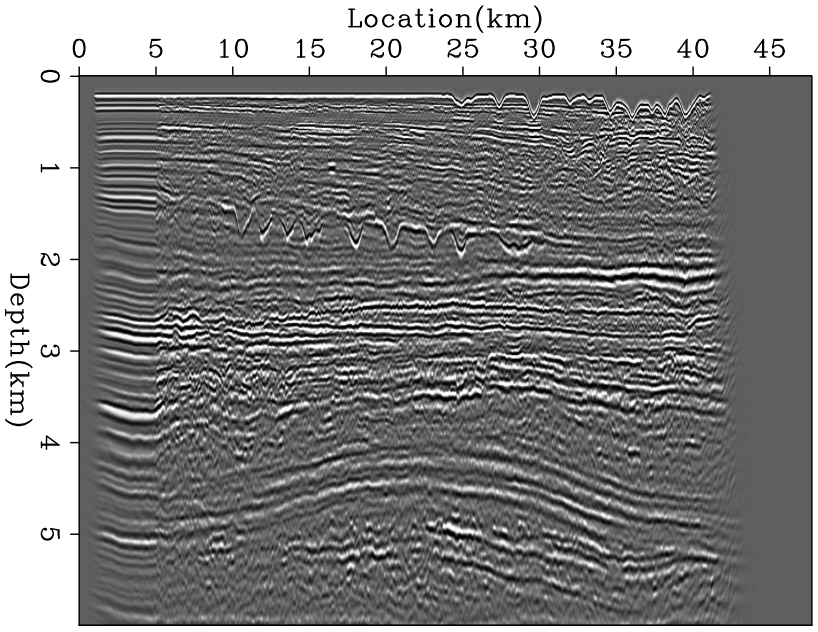

Figure 21: Migration image using the reflection FWI velocity model. [**NR**]

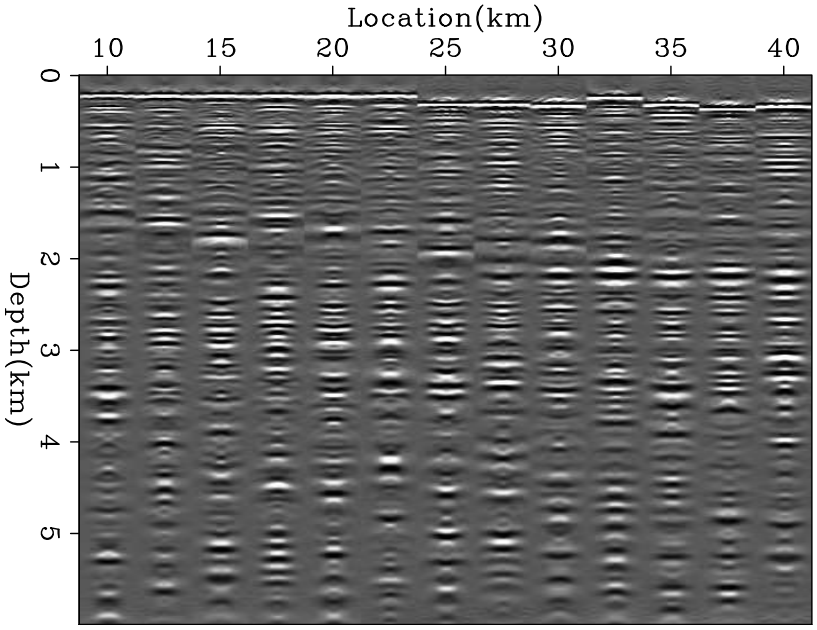

Figure 22: ADCIGs using the reflection FWI velocity model. [**NR**]

CONCLUSIONS

Using the Chevron SEG 2014 synthetic dataset, we estimated the velocity model in a blind FWI test. We first processed the data to enhance the signal-to-noise ratio by bandpassing the useful part of the spectrum and reducing the surface related multiples using the MRKE algorithm. Then, we estimated the velocity in three stages: early-arrival FWI, low-frequency TFWI, and reflection FWI. The early-arrival FWI stage improved the shallow part, the low-frequency TFWI improved the kinematics of the deep part, and the reflection FWI added the reflection information to the model. The migration images as well as the ADCIGs indicate that the final velocity model has successfully estimated the majority of the kinematics in the data. However, we did not fully fit the amplitude due to the difference in physics between the observed data and the modeling operator.

ACKNOWLEDGEMENT

We would like to thank Chevron for providing the dataset and permission to publish the results.

REFERENCES

Almomin, A. and B. Biondi, 2014, Preconditioned tomographic full waveform inversion by wavelength continuation : SEP-Report, **152**, 11–18.

Biondi, B. and A. Almomin, 2014, Efficient and robust waveform-inversion workflow: Tomographic FWI followed by FWI : SEP-Report, **152**, 1–10.

Luo, Y. and G. T. Schuster, 1991, Wave-equation traveltime inversion: Geophysics, **56**, 645–653.

Pratt, R. G., 1999, Seismic waveform inversion in the frequency domain, Part 1: Theory and verification in a physical scale model: Geophysics, **64**, 888–901.

Shen, X., 2014, Early-arrival waveform inversion for near-surface velocity estimation: PhD thesis, Stanford University.

Shen, X., T. Tonellot, Y. Luo, T. Keho, and R. Ley, 2012, A new waveform inversion workflow: Application to near-surface velocity estimation in saudi arabia: SEG Abstracts.

Tarantola, A., 1984, Inversion of seismic reflection data in the acoustic approximation: Geophysics, **49**, 1259–1266.

Woodward, M., 1989, Wave equation tomography: PhD thesis, Stanford University.